



Flow of a blood analogue fluid in a compliant abdominal aortic aneurysm model: Experimental modelling



Valérie Deplano ^{a,*}, Yannick Knapp ^b, Lucie Bailly ^a, Eric Bertrand ^a

^a Aix-Marseille Université, CNRS, Centrale Marseille, IRPHE UMR 7342, F-13384 Marseille, France

^b Université d'Avignon, LAPEC EA4278, F-84000 Avignon, France

ARTICLE INFO

Article history:

Accepted 18 February 2014

Keywords:

Shear thinning fluid
Compliant abdominal aortic aneurysm
In vitro dynamic set-up
Physiological flow
Experimental modelling

ABSTRACT

The aim of this work is to develop a unique *in vitro* set-up in order to analyse the influence of the shear thinning fluid-properties on the flow dynamics within the bulge of an abdominal aortic aneurysm (AAA). From an experimental point of view, the goals are to elaborate an analogue shear thinning fluid mimicking the macroscopic blood behaviour, to characterise its rheology at low shear rates and to propose an experimental device able to manage such an analogue fluid without altering its feature while reproducing physiological flow rate and pressure, through compliant AAA. Once these experimental prerequisites achieved, the results obtained in the present work show that the flow dynamics is highly dependent on the fluid rheology. The main results point out that the propagation of the vortex ring, generated in the AAA bulge, is slower for shear thinning fluids inducing a smaller travelled distance by the vortex ring so that it never impacts the anterior wall in the distal region, in opposition to Newtonian fluids. Moreover, scalar shear rate values are globally lower for shear thinning fluids inducing higher maximum stress values than those for the Newtonian fluids. Consequently, this work highlights that a Newtonian fluid model is finally inadequate to obtain a reliable prediction of the flow dynamics within AAA.

© 2014 Elsevier Ltd. All rights reserved.

1. Introduction

Several biomechanics works have highlighted the particular fluid dynamics occurring within the bulge of an abdominal aortic aneurysm (AAA), especially characterised by the vortex ring generation, propagation, and sometimes impingement on the AAA wall in the distal region (Salsac et al., 2006; Biasetti et al., 2011; Stamatopoulos et al., 2011; Deplano et al., 2013). Besides, the properties of a vortex ring generated by the motion of a piston pushing an amount of fluid in a cylinder through an orifice, have also been extensively studied (Didden, 1979; Saffman, 1995; Couch and Krueger, 2011). However, unlike the asymmetric confined AAA geometry, the majority of these latter studies have investigated vortex ring propagation in semi infinite rigid domains. It is only very recently that (i) Stewart et al. (2012) investigated the vortex ring dynamics in a symmetric confined domain using Newtonian fluids and (ii) Palacios-Morales and Zenit (2013) studied the formation of vortex ring in shear thinning liquids in semi infinite domain. However, the flow conditions consisted in a Dirac velocity waveform, thereby far from the physiological ones which comprise

cycling, deceleration and anterograde part. Moreover, it is well known that AAA geometry involves fluid dynamics yielding to low values of shear rates, less than 1 s^{-1} (Deplano et al., 2013). The hypothesis of blood Newtonian behaviour, usually made in large arteries (Berger and Jou, 2000), is thus not anymore valid. In the macro circulation, the blood main characteristic is its shear thinning behaviour (Mandal, 2005). Numerous *ex vivo* blood characterisation have been done by Chien et al. (1970) and Thurston (1972) for example, to assess the blood rheology in function of various parameters such as hematocrit and temperature. From these experiments, different works have sought to macroscopically mimic the blood behaviour using analogue fluids composed of Xanthane gum dissolved in aqueous solutions of glycerol or of KSCN (Brookshier and Tarbell, 1993; Thurston, 1996; Benard et al., 2007).

Previous experimental studies in large arteries have already investigated flow properties of blood analogue fluids under steady (Gijzen et al., 1999a) but rarely under unsteady flow conditions (Gijzen et al., 1999b). Furthermore, to the authors' knowledge, an *in vitro* experimental device that mimics physiological flow rates and pressures, shear thinning fluid property and, arterial wall's mechanical structural behaviour through a AAA model, has never been developed.

Finally, despite the numerous papers dealing with numerical modelling of AAA's biomechanics, the most recent of them that

* Corresponding author.

E-mail address: deplano@irphe.univ-mrs.fr (V. Deplano).

examined the AAA flow dynamics' difference induced by a Newtonian or a shear thinning fluid (Biasseti et al., 2011) has been realized in a rigid wall AAA geometry, which could change the results. Actually, given the *in vivo* studies showing that the aneurysm wall retains some compliance (Wilson et al., 2001; Long et al., 2005), and the number of numerical works accounting for fluid structure interaction to analyse the AAA's biomechanics (Scotti and Finol, 2007; Rissland et al., 2009), it seems important to consider compliant AAA model.

Therefore, the aim of this work is (i) to define a blood analogue fluid and characterise its rheology at low shear rates, (ii) to propose a unique *in vitro* set-up able to manage such an analogue fluid without altering its feature while reproducing physiological flow rate and pressure waveforms in a compliant AAA geometry and (iii) to determine whether Newtonian fluid model can predict AAA fluid dynamics. This latter goal is achieved by analyzing the influence of the fluid shear thinning behaviour on vortex ring formation and propagation using particle images velocimetry (PIV), and by comparing to that obtained for a Newtonian fluid.

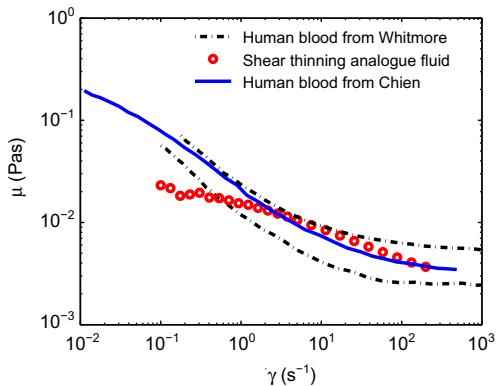


Fig. 1. Experimental dynamic viscosity versus shear rate. \circ , Shear thinning analogue fluid (present work); $- \cdot -$, Corridor of the variations of human blood viscosity from Whitmore (1968), and $-$, Human blood viscosity from Chien et al. (1970).

2. Method

2.1. Characterisation of the working fluids

The target non-Newtonian fluid was characterised by a macroscopic shear thinning behaviour mimicking the blood suspension at standard hematocrit (45%) and body temperature ($T_e = 37^\circ\text{C}$). In order to make this solution compatible with the experimental set-up and the measurement methods, the solution should contain salt for the functioning of electromagnetic flowmeters and should have optical properties suitable with PIV measurements (refractive index and turbidity). Benard et al. (2007) have proven that the addition of Xanthan gum (XG) to aqueous solutions does not affect the solution's refractive index. However, the rheology of such solution is especially sensitive to the addition of salt and, for the concentrations less than 450 ppm, the dynamic viscosity nonlinearly decreases with salt concentration (not shown). Moreover, for XG concentrations above 400 ppm, the solution becomes turbid and PIV measurements delicate. Different proportions of XG, salt, water and glycerol have been tested. Finally, 350 ppm of XG (Δ ries SATIAXANE CX91) with 0.9 g/L sodium salt were added in a distilled aqueous solution of glycerine (20% w/w). The solution rheology was characterised using a Haake III rheometer (Thermo Fisher Scientific) with a cone plate geometry of 60 mm diameter and 2° angle, under constant temperature ($T_e = 25 \pm 0.01^\circ\text{C}$). The fluid testing protocols consisted in 25 levels of shear rates applied step by step in a logarithmic way increasing from 0.1 to 200 s^{-1} followed by a similar decrease. The rheological characterisation of the selected mixture at 25°C shows a behaviour close to that of human blood at $T_e = 37^\circ\text{C}$ and hematocrit of 45% (Fig. 1). The reported viscosity values are mean values obtained during both increasing and decreasing ramps. The relative error at low shear rates (from 0.1 to 1 s^{-1}) was evaluated to 7.5%.

The Newtonian blood analogue behaviour was reproduced using 0.9 g/L sodium salt added in distilled aqueous solution of glycerine (40% v/v). The resulting dynamic viscosity at 25°C was equal to $\mu_N = 4.039\text{cP}$ and its density, $\rho_N = 1099\text{ kg/m}^3$.

2.2. Experimental set-up and measurements

The experimental arrangement has been designed to preserve the selected fluid properties and the conformation of its molecular chains during the dynamics experiments. This results in a circulating fluid temperature control, the exclusion of any metallic element and of stresses of the flowing fluid generated by the pumping system. The set-up was therefore composed of three interacting mock loops (Fig. 2).

(1) The circulatory loop contains the working fluid flowing from an open tank through flexible left atrium and ventricle models, an upstream compliant element, the AAA model, a downstream windkessel model, to finally return into the open tank. A silicone 3-leaflets valve separates the left atrium and ventricle to mimic the mitral valve. Another identical valve, mimicking the aortic valve, is located at the ventricle outlet. The systemic arterial tree is reproduced by the downstream

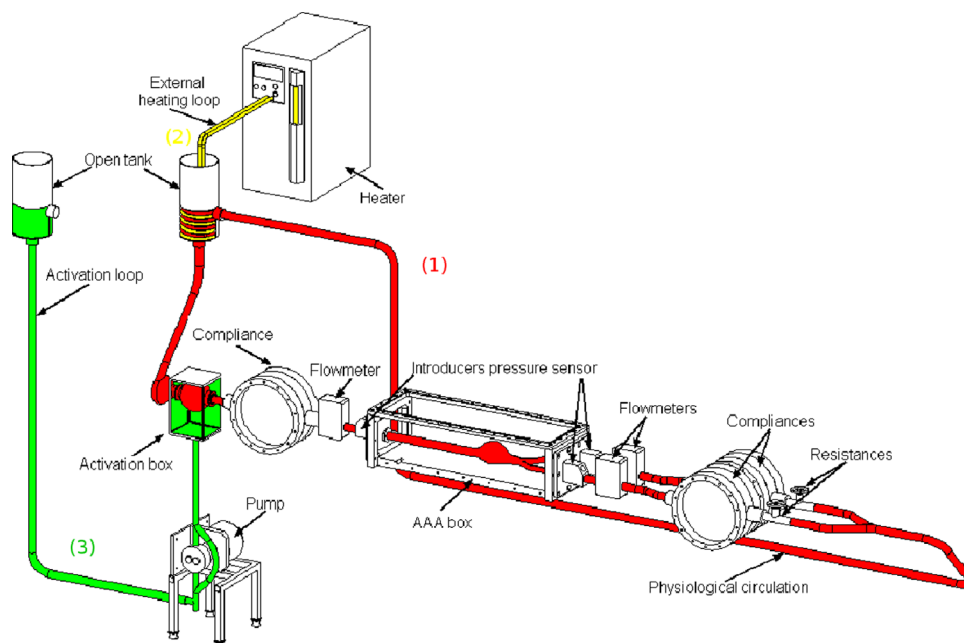


Fig. 2. Experimental set-up. (1) Circulatory loop; (2) heating/cooling loop; and (3) activation loop.

windkessel model which comprises a compliance and a resistance while the antegrade portion of the flow rate is controlled by the upstream compliance. The AAA model is immersed in a transparent box filled with the selected working fluid, which gives flat optical access with minimum optical distortion. This box also allows to control the distensibility of the AAA model.

(2) The heating/cooling loop enables to control the selected working fluid temperature. An external system pumps water through a heat exchanger located in the open tank of the circulatory loop. Several thermocouples are inserted at various locations of the circulatory loop to control the temperature.

(3) The activation loop contains water, pumped from an open tank into a closed box including the left ventricle model. Pumping the water in and out of this box, thanks to a specific computer controlled gear pump, insures a contractile motion of the ventricle resulting in physiological flow conditions in the circulatory loop.

The AAA geometrical model (Fig. 3) was described in Deplano et al. (2013). Briefly, the AAA bulge was asymmetric through its anterior posterior (AP) plane. Without loading, the maximum lateral diameter of the AAA, D_L , was equal to 6.48 cm and the maximum AP diameter, D_{AP} , to 5.46 cm. The length of the AAA, L_{AAA} , was equal to 11.8 cm. The inlet tube diameter, D_{in} , was equal to 2.1 cm and the iliac artery diameters were equal to 1.3 cm. The AAA geometrical model was made of moulded Estane®5714 (Meyer et al., 2011). Its mechanical characterisation, through Peterson modulus (E_p) evaluation, has been described in Deplano et al. (2013) and has highlighted that Estane offers similar structural mechanics behaviour to that of a real AAA.

The instantaneous flow rates and pressure were measured by electromagnetic flowmeters (Gould Statham SP2202) and Millar catheters (MPC 500) respectively. The *in vivo* human flow rate derived from Olufsen et al. (2000) (Fig. 4). At infinite shear, the maximum flow rate, Q_{max} , was equal to 7.09 L/min and the maximum Reynolds number, $Re_{max} = \frac{U_{max} D_{in}}{\nu_N}$ to 1941. The period of the flow rate, T , was equal to 0.938 s, so that the frequency parameter $\alpha = \frac{D_{in}}{2} \sqrt{\frac{2\pi}{T\nu_N}}$ was equal to 14.17. The E_p value was equal to 3.8×10^5 Pa. Both outlet flow division at the branches (right to left iliac arteries) was set to 50% 50%. The inlet flow rate and E_p were kept constant whatever the working fluid.

The velocity field was obtained using PIV system. The flow was seeded with 15–20 μm nylon particles with the same density as the working fluid. This density matching prevented floating or sedimentation of the particles. The flow was illuminated by a 1 mm thick sheet of laser generated by a double pulsed mini Yag laser (NewWave, 120 mJ) and images were acquired with a CCD camera (Powerview Plus 2MP). The measurements were carried out in the AP plane of the AAA, at 20 instants during the cycle separated by 50 ms. The time delay

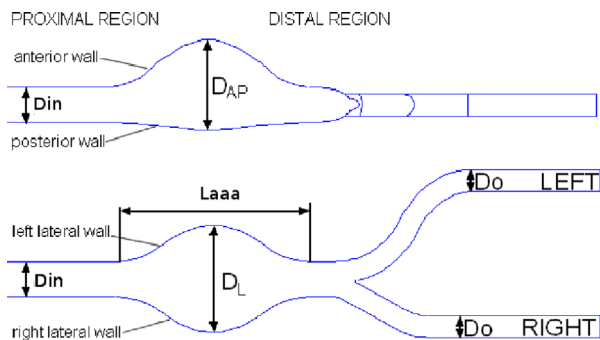


Fig. 3. Geometrical model diagram. First line AP plane and second line perpendicular plane to AP plane.

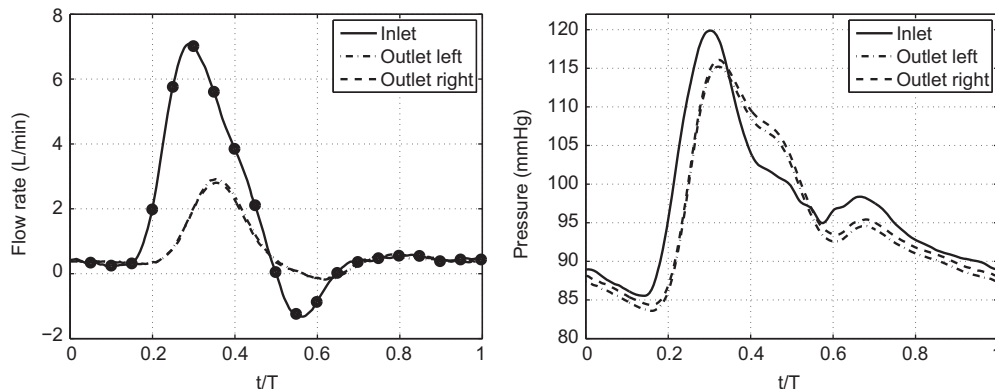


Fig. 4. Inlet (solid lines) and outlet (dotted lines) flow rate (left) and pressure (right) waveforms versus nondimensional time t/T for Newtonian case. The black circles represent the 20 recorded instants.

between two laser pulses was set to 1200 μs . The acquisition of 80 PIV image pairs at each instant, was triggered by the pump signal. To obtain higher spatial resolution, a recursive two steps Nyquist grid algorithm was implemented. During the first step, cross-correlations were computed on 32×32 pixels, 50% overlapping interrogation windows. The second computation of cross-correlation was performed on 16×16 pixels interrogation windows resulting in $0.77 \times 0.77 \text{ mm}^2$ final spatial resolution.

3. Results

For Newtonian fluid, the description and quantification of the vortex ring (VR) propagation and impingement onto the distal anterior wall of the AAA bulge have been described in Deplano et al. (2013). Therefore, in the following, emphasis is accorded to the comparison between Newtonian and shear thinning fluids.

The vorticity values were computed from the PIV velocity fields and were defined as $\omega = \frac{1}{2} (\frac{\partial v}{\partial x} - \frac{\partial u}{\partial y})$, where u , v , x and y are the axial and transverse velocity components and axes respectively.

A vortex identification scheme (Zhou et al., 1999) using the λ_{ci} criterion was employed to distinguish the vortex cores from vorticity regions generated at the confinement walls or at the shear layers. Based on this criterion, several quantities were computed: the vorticity values at the VR cores, the VR propagation velocity, the travelled distance by the VR, the VR circulation strength and the AP radius of the VR.

3.1. Vorticity

The vorticity maps are presented versus non-dimensional time, $T_a = t/T$ in Fig. 5, which shows the VR intersections with the AP plane, referred by anterior and posterior part. For both fluids, because of the asymmetry of the AAA enlargement in the AP plane, the VR is stretched as demonstrated by the posterior part ahead the anterior one. Although the VR detachment from the proximal neck occurs approximately at the same instant of the cycle, $T_a = 0.398$ (Fig. 5, line 3), its downstream convection for the shear thinning case is slower than for the Newtonian one. Moreover, for the Newtonian fluid, the VR impinges on the anterior wall in the distal AAA region around $T_a = 1 + 0.548$, whereas it is still in the AAA bulge for the shear thinning fluid at that time (Fig. 5, lines 4 and 5). For shear thinning fluid the vortex ring never impacts the distal wall. Therefore, for shear thinning fluid, at $T_a = 1 + 0.548$, there is no increase of the boundary layer vorticity values on the distal anterior wall (Fig. 5, line 4). In the same way, for the Newtonian case, at $T_a = 1 + 0.7$, the posterior part of the VR moves towards the distal AAA neck inducing an increase of the boundary layer vorticity values at this neck that does not occur for shear thinning fluid (Fig. 5, line 5). It is also important to notice that

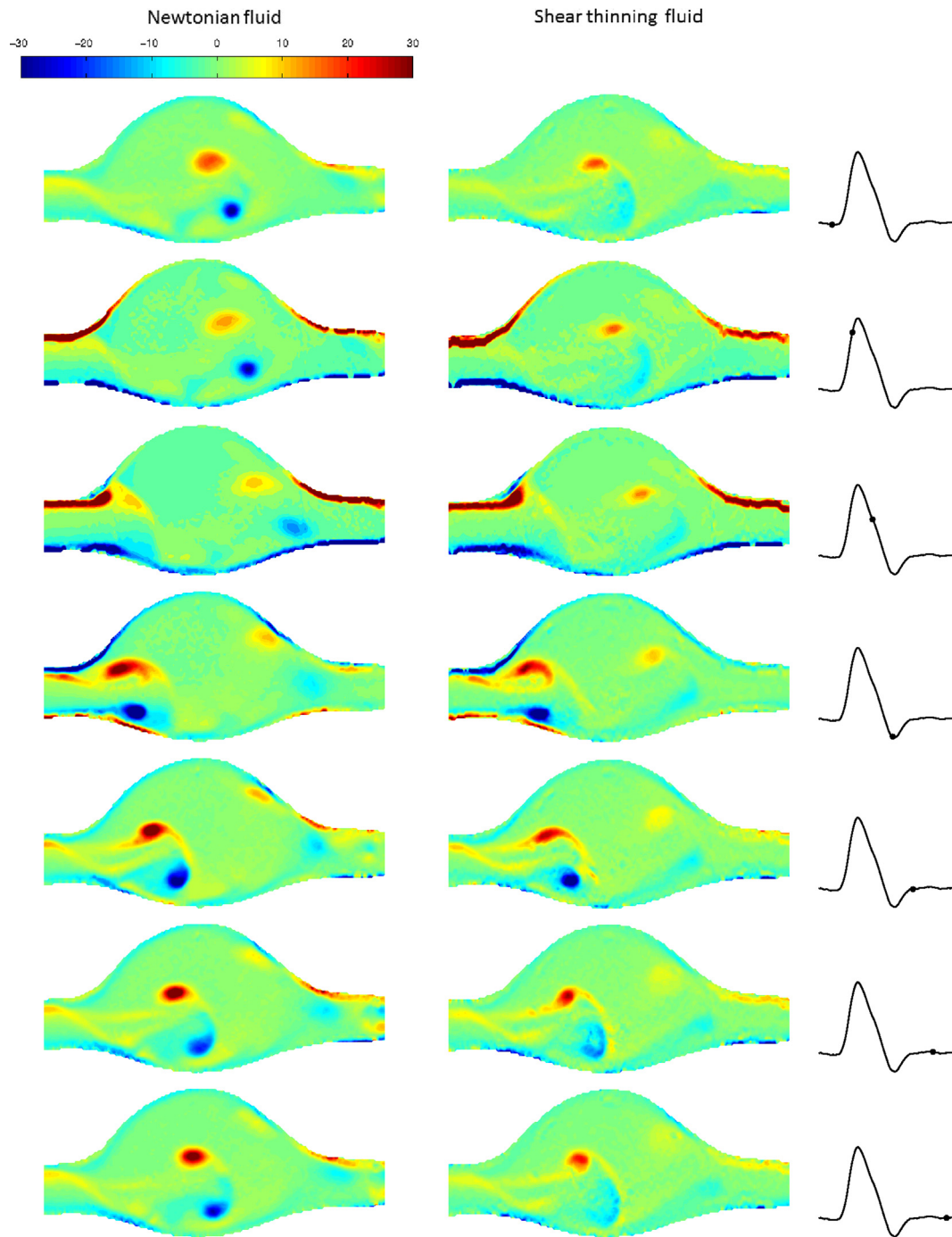


Fig. 5. Vorticity maps in s^{-1} in the AP plane versus non-dimensional time : $T_a=0.1, 0.245, 0.398, 0.548, 0.7, 0.8475,$ and 0.946 .

within a cycle from $T_a=0.8475$, the posterior part vorticity values in the VR of the shear thinning fluid are much lower than the Newtonian ones, about 2.66 times.

3.2. Vortex ring propagation

During a cycle starting from the VR detachment from the proximal neck, the evolution of the VR propagation velocity, (Fig. 6, left), exhibits a general trend similar for both fluids with an increase over a short first phase of the cycle, followed by a decrease over the remaining part of the cycle. However, the relative difference between Newtonian and shear thinning fluid is equal to 27.8% on average. Due to the viscous dissipation, the shear thinning evolution also shows less oscillations than the

Newtonian ones. When considering the travelled distance by the VR (Fig. 6, right) the behaviours are quite similar for both fluids until $T_a=0.59$, afterwards the deviation increases with time. The relative difference between Newtonian and shear thinning fluid is equal to 12.8% on average. At the end of the considered period, the anterior part of the VR reaches 46% of the AAA length for the shear thinning fluid versus 53% for the Newtonian one. Therefore both VR velocities and travelled distance values decrease with thinning property of the working fluid.

3.3. Circulation strength

The circulation strength (Fig. 7, left) of the VR intersection with the AP plane was determined by integrating the vorticity over the

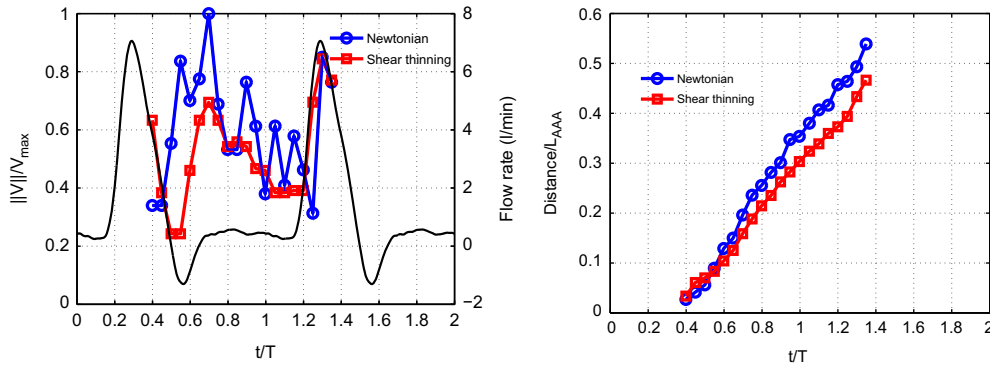


Fig. 6. Comparison of the VR velocity propagation of the anterior part of the VR, nondimensioned by the maximum Newtonian velocity propagation encountered in the cycle (left) and of the travelled distance of the anterior intersection of the VR, non-dimensioned by the AAA length (right). Newtonian (\circ) fluid; shear thinning (\square).

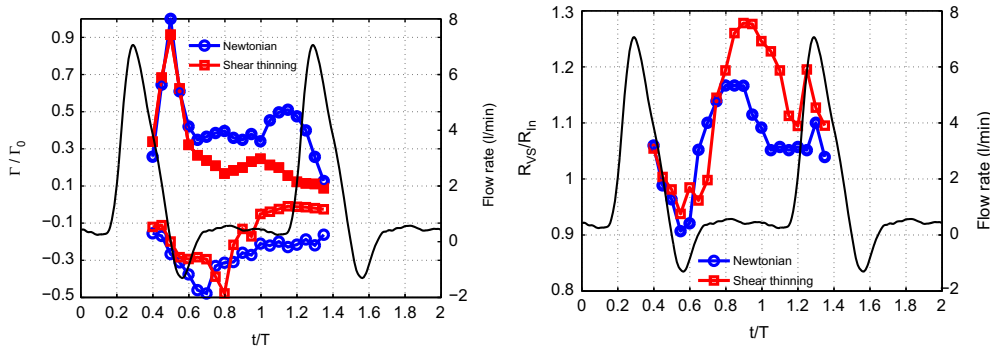


Fig. 7. Left: Comparison of Γ non-dimensioned by its Newtonian maximum value Γ_0 ; \circ and \bullet for Newtonian anterior and posterior respectively, \square and \blacksquare for shear thinning anterior and posterior respectively. Right: comparison of anterior–posterior radius of the VR non-dimensioned by R_{in} ; \circ for Newtonian and \square for shear thinning.

area (A) identified by $\lambda_{ci} = 10\%$ of the maxima values occurring within the cardiac cycle for each fluid so that $\Gamma = \int_A \omega \, dx \, dy$. The variations between the anterior and posterior circulation strength are caused by the asymmetry of the AAA enlargement in the AP plane; the wall confinement is greater on the side of the posterior wall.

The global waveforms of the circulation strength are similar for both fluids. Considering the anterior part, during the decelerating phase of the flow rate, the VR detachment generates an increase of the circulation strength just before the maximum of the anterograde flow rate is reached. As the VR propagates further, the circulation strength first decays notably due to the geometric confinement; the core vorticity decreases (not shown) and correspondingly the AP radius of the VR grows (Fig. 7, right). These results are in agreement with the literature on confined vortex ring (Stewart et al., 2012). After this first decrease, the circulation strength increases again; correspondingly the AP radius of the VR diminishes.

The evolution of the posterior part shows an increase of the circulation strength amplitude until the flow rate becomes approximately constant, followed by a decrease until the end of the considered period.

The values measured for the Newtonian fluid are 1.89 and 5.44 times greater than those of shear thinning fluid for the anterior posterior part respectively. In fact, the shear thinning posterior part circulation strength values are close to zero from $T_a = 1$.

This result is in agreement with Palacios-Morales and Zenit (2013) who observed that the vortex circulation strength decreases considering shear thinning fluid in semi infinite domain. In addition, except for the maximum anterior circulation which occurs simultaneously for both fluids, the evolution of the curves puts into light a phase shift.

3.4. Shear related quantities

The scalar shear rate, $\dot{\gamma} = \sqrt{2e : e}$, which is an invariant of the strain rate tensor $e = \frac{1}{2}(\nabla U + \nabla U^t)$ was plotted in Fig. 8. Maximum stress, τ_{max} , defined as the maximum eigenvalue of the stress tensor $\tau = 2\mu(\dot{\gamma})e$, was plotted in Fig. 9. Until the VR detaches, the largest scalar shear rate and maximum stress values, $\dot{\gamma} > 35 \, \text{s}^{-1}$ and $\tau_{max} > 0.2 \, \text{Pa}$, are confined to the boundary layers, whereas during VR propagation they move into the AAA bulge around the vortex ring. The maxima Newtonian fluid scalar shear rate values are higher than the shear thinning ones. However, when $\dot{\gamma}$ drops below $30 \, \text{s}^{-1}$, $\mu(\dot{\gamma})$ is higher for shear thinning fluid, so that during the VR propagation the values of τ_{max} are greater for shear thinning fluid.

3.5. Particle trajectories

Although the flow is 3D and the AAA model is asymmetric, a particle tracking algorithm was applied on the data obtained in the AP plane (Appendix A). This plane is a symmetry plane of the geometrical model so that the tracking algorithm should provide a relatively good approximation of the particle trajectories. This assumption is also supported by the fact that the flow in the AP perpendicular plane remains symmetric with respect to the AP plane (Deplano et al., 2013).

Particle–particle collisions are neglected and particle motion does not act on the flow field. When a particle impacts the wall, it vanishes. The hypothesis that the particles follow the flow is retained as the Stokes number, St , is negligible compared to unity (Appendix A).

The trajectories of particles depend on the fluid rheology. In order to easily illustrate the difference of the particle trajectories between Newtonian and Non-Newtonian fluid, 8 particles, released at $T_a=0$ from two different emission lines, are plotted (Fig. 10) considering 10 cardiac cycles. For Newtonian fluid, when particles are released close to the anterior wall in the distal region (Fig. 10a), they follow the anterior wall with a backward motion, skirt the central region of AAA bulge, some impact the anterior wall but also the posterior wall close of the AAA centre, others are trapped close the proximal neck and few of them flow away the AAA bulge. For shear thinning fluid, as the VR never impacts the

anterior wall, the particles motions are mainly concentrated in the upper part of the AAA bulge, some are deflected to the posterior wall, yet further than the Newtonian case and without impingement, more particles leave the AAA.

When particles are released near the top of the bulge (Fig. 10b) for Newtonian fluid, they again skirt the central region of AAA bulge, remain concentrated close to the proximal neck, some are shifted to the posterior and few of them leave the AAA. For shear thinning fluid, several particles leave the AAA after being concentrated in the proximal part of the AAA bulge. The shear thinning fluid submits the particles to τ_{max} values 2 times greater than the Newtonian fluid.

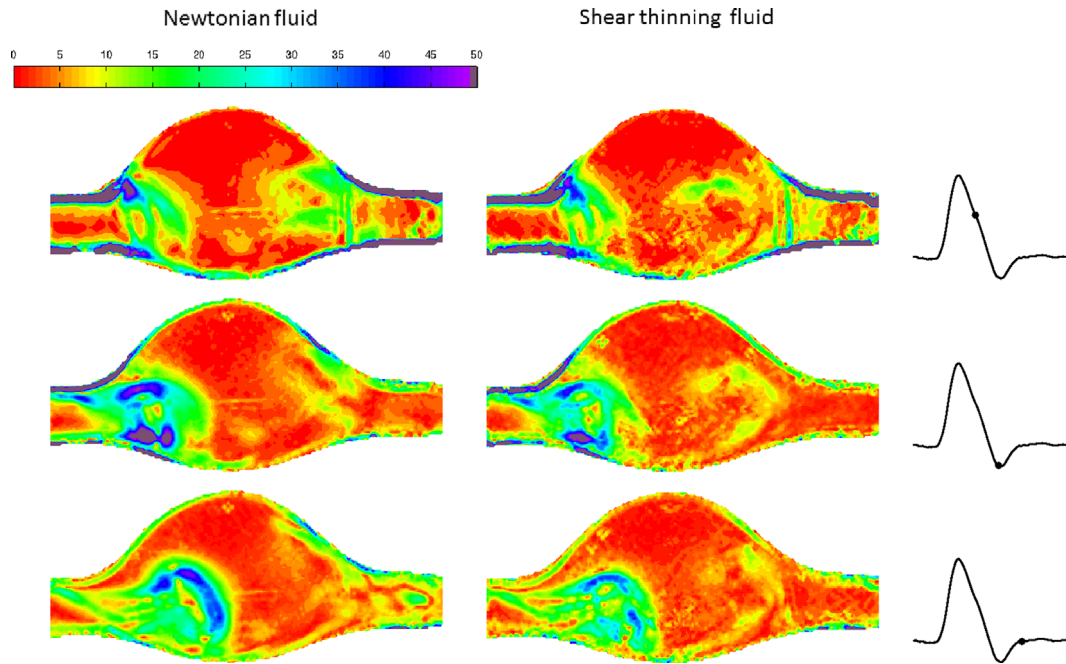


Fig. 8. Scalar shear rate, $\dot{\gamma}$ in s^{-1} , versus non-dimensional time in the AP plane. $T_a=0.398, 0.548, \text{ and } 0.7$.

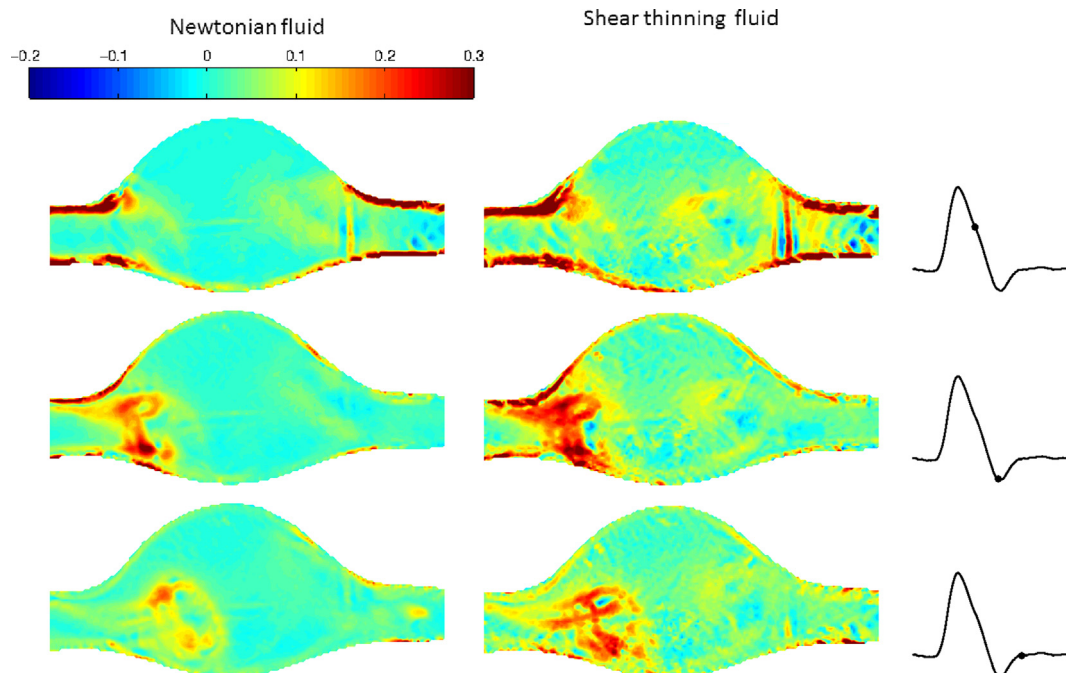


Fig. 9. Maximum stress values, τ_{max} in Pa versus non-dimensional time in the AP plane. $T_a=0.398, 0.548, \text{ and } 0.7$.

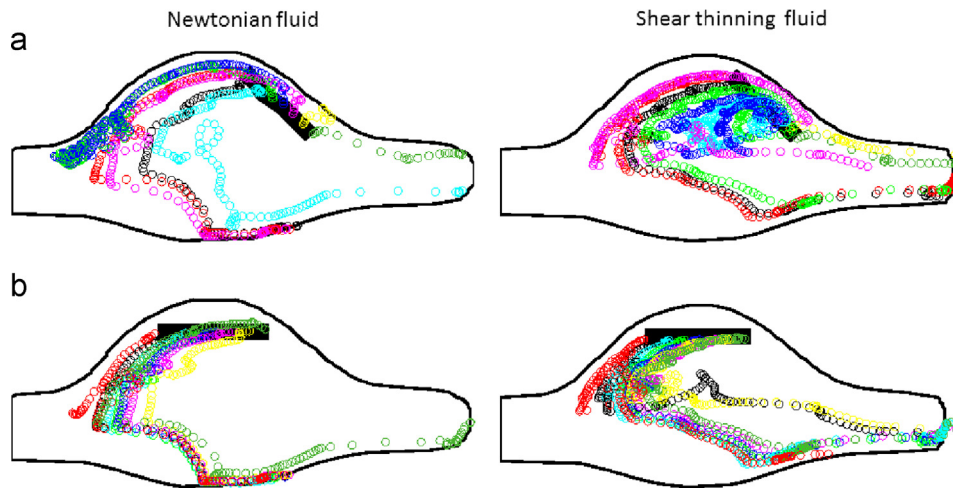


Fig. 10. Tracking of 8 particles during 10 cardiac cycles. Particles were initially located (a) close to anterior wall called emission line n°1 and (b) close to the top of the AAA bulge, called emission line n°2. Emission lines are represented by thick black line.

4. Discussion and conclusion

For the first time in the literature, a unique *in vitro* set-up, considering compliant aneurysm model, able to manage a blood analogue fluid without altering its feature while reproducing physiological flow conditions has been successfully designed. This experimental device was used to analyse the influence of fluid shear thinning behaviour on VR features and propagation. The main results have highlighted that (i) the propagation velocity of the VR is slower for shear thinning fluid inducing smaller travelled distance by the VR, (ii) in opposition to Newtonian fluid, the VR never impacts the anterior wall for shear thinning fluid, (iii) whatever the time in the cycle, the vortex circulation strength values are much smaller for shear thinning fluid, inducing notably higher anterior posterior vortex radius during one half of the cardiac cycle, (iv) scalar shear rate values are mainly lower for shear thinning fluid so that maximum stress values are mainly higher than those for the Newtonian fluid, and (v) different preferred areas of concentration of particles are predicted depending on the fluid rheology.

To summarize, the flow dynamics is highly dependent on the fluid rheology. Consequently, taking into account fluid structure interaction, this experimental work highlights that a Newtonian fluid model is finally inadequate to obtain a reliable prediction of the flow dynamics within AAA. This new experimental device could be used to validate complex numerical modellings.

It is known that the flow dynamics plays a role in the AAA biomechanical processes, especially in the formation of intra luminal thrombus (ILT). Few works dealt with fluid dynamics mechanism of ILT formation through platelets activation, convection and deposition (Basciano et al., 2011; Biasetti et al., 2011; O'Rourke et al., 2012). The main reported concept is that the vortex ring traps platelets, transports them during its propagation from the proximal to the distal neck and releases them during its break-up. The platelets are activated during their stay in the vortex ring due to high shear stress and/or high residence times so that they can aggregate and/or adhere to the AAA wall at low wall shear stress sites. The results obtained in this study show that shear thinning fluid model induces higher maximum stress values than for Newtonian model which implies an *a priori* favourable configuration for platelet activation. Moreover, although particles seem to leave the AAA bulge more quickly for the shear thinning fluid, most of them are likely recirculated in the upper central part of the AAA bulge in opposition to Newtonian model. However, for shear thinning fluid, the vortex ring does not reach the distal AAA wall.

It is therefore difficult to conclude that platelets can adhere to the AAA wall. Furthermore, VR dynamics is, among other reasons, driven by the magnitude and the waveforms of the flow rate and pressure, the AAA confinement ratio, and the tortuosity of the AAA geometry. Therefore, further investigations have to be performed to confirm or invalidate the influence of the VR dynamics on ILT formation.

The present work has some limitations. The XG blood analogue solution does not mimic the higher blood viscosity values for lower shear rates. It is important to notice that for higher viscosity values the flow dynamics differences between Newtonian and shear thinning will be more important, so that the result obtained in this work would not be invalidated but would be enhanced. Moreover, the model does not include thrombus. The presence of ILT induces geometrical changes that can modify the AAA flow field and change the AAA biomechanics. Modeling of ILT is of primary interest but was beyond the scope of the present experimental set-up. However, this study can participate to highlight biomechanical processes implied in its development.

Conflict of interest statement

All authors declare that there are no conflicts of interest.

Appendix A. Supplementary material

Supplementary data associated with this article can be found in the online version at <http://dx.doi.org/10.1016/j.jbiomech.2014.02.026>.

References

- Basciano, C., Kleinstreuer, C., Hyun, S., Finol, E.A., 2011. A relation between near-wall particle hemodynamics and onset of thrombus formation in abdominal aortic aneurysms. *Ann. Biomed. Eng.* 39 (7), 2010–2026.
- Biasetti, J., Hussain, F., Gasser, T.C., 2011. Blood flow and coherent vortices in the normal and aneurysmatic aortas: a fluid dynamics approach to intra-luminal thrombus formation. *J. R. Soc. Interface* 8, 1449–1461.
- Benard, N., Jarny, S., Coisne, D., 2007. Definition of an experimental blood like fluid for laser measurements in cardiovascular studies. *Appl. Rheol.* 17, 44151-1–44251-8.
- Berger, S.A., Jou, L.D., 2000. Flows in stenotic vessels. *Ann. Rev. Fluid Mech.* 32, 347–382.
- Brookshier, K.A., Tarbell, J.M., 1993. Evaluation of a transparent blood analog fluid: aqueous xanthan gum/glycerine. *Biorheology* 30, 107–116.
- Couch, L.D., Krueger, P.S., 2011. Experimental investigation of vortex rings impinging on inclined surfaces. *Exp. Fluids* 51, 1123–1138.

- Chien, S., Usami, S., Dellenback, R.J., Gregersen, M.I., 1970. Shear-dependent deformation of erythrocytes in rheology of human blood. *Am. J. Physiol.* 219, 136–142.
- Deplano, V., Meyer, C., Guivier-Curien, C., Bertrand, E., 2013. New insights into the understanding of flow dynamics in an in vitro model for abdominal aortic aneurysms. *Med. Eng. Phys.* 35, 800–809.
- Didden, N., 1979. On the formation of vortex rings: rolling-up and production of circulation. *Z. Angew. Math. Phys.* 30 (1), 101–116.
- Gijzen, F.J.H., Van de Vosse, F.N., Janssen, J.D., 1999a. The influence of the non-Newtonian properties of blood on the flow in large arteries: steady flow in a carotid bifurcation model. *J. Biomech.* 32, 601–608.
- Gijzen, F.J.H., van de Vosse, F.N., Janssen, J.D., 1999b. The influence of the non-Newtonian properties of blood on the flow in large arteries: unsteady flow in a 90° curved tube. *J. Biomech.* 32, 705–713.
- Long, A., Rouet, L., Bissery, A., Rossignol, P., Mouradian, D., Sapoval, M., 2005. Compliance of abdominal aortic aneurysms evaluated by tissue Doppler imaging: correlation with aneurysm size. *J. Vasc. Surg.* 42, 18–26.
- Mandal, P.K., 2005. An unsteady analysis of non-Newtonian blood flow through tapered arteries with a stenosis. *Int. J. Non-Linear Mech.* 40, 151–164.
- Meyer, C., Bertrand, E., Boiron, O., Deplano, V., 2011. Stereoscopically observed deformations of a compliant abdominal aortic aneurysm model. *J. Biomech. Eng. Trans. ASME* 133 (11), 111004.
- Olufsen, M.T., Peskin, C.S., Kim, W.Y., Pedersen, E.M., Nadim, A., Larsen, J., 2000. Numerical simulation and experimental validation of blood flow in arteries with structured-tree outflow conditions. *Ann. Biomed. Eng.* 28, 1281–1299.
- O'Rourke, M.J., McCullough, J.P., Kelly, S., 2012. An investigation of the relationship between hemodynamics and thrombus deposition within patient-specific models of abdominal aortic aneurysm. *Proc. Inst. Mech. Eng.: Part H: J. Eng. Med.* 226 (7), 548–564.
- Palacios-Morales, C., Zenit, R., 2013. The formation of vortex rings in shear-thinning liquids. *J. Non-Newton. Fluid Mech.* 194, 1–13.
- Rissland, P., Alemu, Y., Einav, S., Ricotta, J., 2009. Abdominal aortic aneurysm risk of rupture: patient-specific FSI simulations using anisotropic model. *J. Biomech. Eng.*, 131.
- Saffman, P.G., 1995. *Vortex Dynamics*. Cambridge University Press, Cambridge.
- Salsac, A.V., Sparks, R.R., Chomaz, J.M., Lasheras, J.C., 2006. Evolution of the wall shear stresses during the progressive enlargement of symmetric abdominal aortic aneurysms. *J. Fluids Mech.* 560, 19–51.
- Scotti, C.M., Finol, E.A., 2007. Compliant biomechanics of abdominal aortic aneurysms: a fluid–structure interaction study. *Comput. Struct.* 85, 1097–1113.
- Stamatopoulos, Ch., Mathioulakis, D.S., Papaharilaou, Y., Katsamouris, A., 2011. Experimental unsteady flow study in a patient-specific abdominal aortic aneurysm model. *Exp. Fluids* 50, 1695–1709.
- Stewart, K.C., Niebel, C.L., Jung, S., Vlachos, P.P., 2012. The decay of confined vortex rings. *Exp. Fluids* 53, 163–171.
- Thurston, G.B., 1972. The viscoelasticity of human blood. *Biophysical. J.* 12, 1205–1217.
- Thurston, G.B., 1996. Viscoelastic properties of blood and blood analogs. In: How T.V. (Ed.), *Advances in Haemodynamics and Haemorheology*, JAI Press, Inc.
- Zhou, J., Adrian, R., Balachandar, S., Kendall, T.M., 1999. Mechanisms for generating coherent packets of hairpin vortices in channel flow. *J. Fluids Mech.* 387, 353–396.
- Wilson, K.A., Lindholt, J.S., Hoskins, P.R., Heickendorff, L., Vammen, S., Bradbury, A.W., 2001. The relationship between abdominal aortic aneurysm distensibility and serum markers of elastin and collagen metabolism. *Eur. J. Vasc. Endovasc. Surg.* 21, 175–178.
- Whitmore, 1968. *Rheology of the Circulation*. Pergamon Press, Oxford.